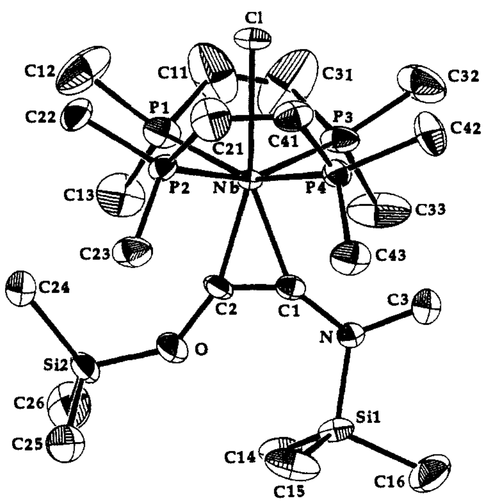

Figure 1. ORTEP diagram of **2** showing the 40% probability thermal ellipsoids. Hydrogen atom positions were calculated. Selected bond distances (Å) and angles (deg) are as follows: Nb–C1, 2.125 (7); Nb–C2, 2.079 (7); C1–C2, 1.30 (1); C1–N, 1.386 (9); C2–O, 1.385 (8); N–C3, 1.47 (1); N–Si1, 1.744 (6); O–Si2, 1.615 (6); Nb–P1, 2.573 (2); Nb–P2, 2.554 (2); Nb–P3, 2.562 (2); Nb–P4, 2.545 (2); Nb–Cl, 2.586 (1); C1–Nb–C2, 35.9 (3); Nb–C2–O, 158.7 (5); Nb–C1–N, 149.5 (5); C2–O–Si2, 140.3 (6); C1–N–Si1, 120.9 (5); Cl–N–C3, 118.8 (6); P1–Nb–P3, 76.93 (8); P1–Nb–P2, 98.74 (7).

were consistent with the formula $[\mathrm{Nb\{(Me_3Si)(Me)NCCO(SiMe_3)\}(dmpe)_2Cl}]$ (**2**), in which C≡O and C≡NR are reductively coupled to form a highly functionalized acetylene (eq 3).

$$[\mathrm{Nb(CNMe)(CO)(dmpe)_2Cl}] \xrightarrow{40\%\ \mathrm{Na/Hg}} \xrightarrow{2\mathrm{Me_3SiCl}} [\mathrm{Nb\{(Me_3Si)(Me)NCCO(SiMe_3)\}(dmpe)_2Cl}] \quad (3)$$

The structure of **2** (Figure 1) was revealed by X-ray analysis of a green single crystal grown from pentane at -20 °C.[13] The geometry is distorted octahedral with the midpoint of the acetylene defining one vertex. The dmpe ligands are in an asymmetric envelope conformation[14] with the methylene linker chains pointing toward the chlorine atom. The coordinated RR′NC≡COR moiety is planar, indicating a delocalized electronic structure.[15] The acetylene is bound asymmetrically, however, with the Nb–C1 bond distance being 0.05 Å greater than that of Nb–C2. The difference indicates that resonance form ii plays a significant role in metal–ligand bonding. Functionalized acetylenes of the form RR′NC≡COR have not been isolated.[16] Although there are several examples of the symmetric, metal-coordinated substituted acetylenes ROC≡COR[1,17] and RR′NC≡CNRR′,[10,15a,18] to our knowledge **2** is the first example of the mixed RR′NC≡COR acetylene ligand.

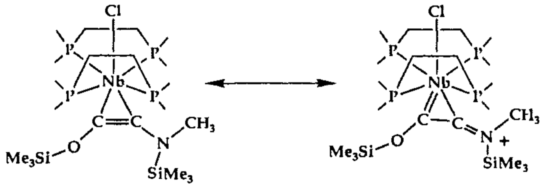

i ii

In summary, reductive coupling of linear triply bonded ligands in seven-coordinate early transition metal complexes has been extended in a significant way to the cross-coupling of C≡O and C≡NR. This work demonstrates the generality of the reaction mechanism previously elucidated for both the isocyanide and carbon monoxide coupling schemes.

Acknowledgment. This work was supported by a grant from the National Science Foundation. We thank Dr. R. N. Vrtis and Professor R. L. Danheiser for helpful discussions.

Supplementary Material Available: Tables of atomic positional and thermal parameters for **2** (5 pages). Ordering information is given on any current masthead page.

---

(12) Anal. Calcd for $C_{21}H_{53}NOSi_2P_4ClNb$ (**2**): C, 39.16; H, 8.29; N, 2.17. Found: C, 39.31; H, 7.67; N, 2.41. FTIR (KBr) 2960, 2897, 2802, 1550, 1420, 1396, 1243, 1147, 1086, 1003, 935, 889, 846, 752, 718, 680, 611, 447 cm^{-1}. ^{1}H NMR (300 MHz, C_6D_6): δ 1.65 (br, PCH_2), 1.58 (br, PCH_3), 1.22 (Br, PCH_2), 1.13 (br, PCH_3), 0.46 (SiMe_3), 0.19 (SiMe_3) ppm.

(13) Crystal data (-70 °C) for **2**: $C_{21}H_{53}NOSi_2P_4ClNb$, $M_r = 644.1$, monoclinic, space group $P2_1$ (No. 4), $a = 10.204$ (5) Å, $b = 18.475$ (1) Å, $c = 9.776$ (5) Å, $\beta = 115.51$ (2)°, $Z = 2$, $V = 1663$ (1) Å^3, $\rho_{\mathrm{calcd}} = 1.29$ g cm^{-3}. For 2870 unique reflections with $F^2 > 3\sigma(F^2)$, $R = 0.034$ and $R_w = 0.042$. Inversion of the coordinates and refinement of the other enantiomorph did not alter the R factors.

(14) Hawkins, C. J. *Absolute Configuration of Metal Complexes*; John Wiley & Sons: New York, 1971.

(15) (a) Corfield, P. W. R.; Baltusis, L. M.; Lippard, S. J. *Inorg. Chem.* **1981**, *20*, 922. (b) Templeton, J. L.; Herrick, R. S.; Morrow, J. R. *Organometallics* **1984**, *3*, 535. (c) See also ref 10.

(16) (a) Viehe, H. G., Ed. *Chemistry of Acetylenes*; Marcel Dekker: New York, 1969. (b) CAS ONLINE structure search for complexes (OC≡CN), 1967 to present.

(17) Vrtis, R. N.; Rao, C. P.; Bott, S. G.; Lippard, S. J. *J. Am. Chem. Soc.* **1988**, *110*, 7564.

(18) Chisholm, M. H.; Ho, D.; Huffman, J. C.; Marchant, N. S. *Organometallics* **1989**, *8*, 1626.

State-Selected Mobilities of Atomic Cobalt Ions

P. R. Kemper and M. T. Bowers*

Department of Chemistry, University of California
Santa Barbara, California 93106

Received January 16, 1990

Studies of the reactivities of first row transition metal ions have shown the ion–neutral interaction to be complex and usually extremely dependent on the metal ion electronic state.[1-8] In recent experiments, we have found a striking effect in our measurement of Co^+ mobility in He. The arrival-time distribution (ATD) for Co^+ is bimodal, suggesting that two different electronic states are involved with very different interactions with He. This observation is interesting for at least three reasons. First, only one other first row transition metal ion mobility has been measured (ground state Ti^+).[9] Second, our results allow us to perform state-specific chemistry, since known and variable populations of ground- and excited-state ions can be produced and detected.[10] Third, it increases our understanding of Co^+ reactivity, allowing separation of effects common to all Co^+–neutral interactions and those specific to a particular system.

The Co^+ ions in our experiment[11] are formed by low-pressure electron impact of $Co(CO)_3NO$ (I) and cyclopentadienylcobalt dicarbonyl (II). The ions are mass selected and injected into a high-pressure gas cell. The ions are quickly translationally thermalized by collisions with He ($P_{\mathrm{He}} \sim$ 1–2 Torr).[11] A small electric field drifts the ions through the cell (E/N = 2–6 Td). Ions exit the cell and are quadrupole mass analyzed and collected. In the mobility experiments,[11] ions are pulsed into the cell and the

---

(1) (a) *Gas Phase Inorganic Chemistry*; Russell, D. H., Ed.; Plenum: New York, 1989. (b) For a nice review of the current state of the field, see: Armentrout, P. B. Electronic State-Specific Transition Metal Ion Chemistry. *Annu. Rev. Phys. Chem.*, in press.

(2) Tonkyn, R.; Ronan, M.; Weisshaar, J. C. *J. Phys. Chem.* **1988**, *92*, 92 and references therein.

(3) (a) Saunders, L.; Hauton, S.; Weisshaar, J. C. *J. Phys. Chem.* **1987**, *91*, 5145. (b) Hauton, S.; Saunders, L.; Weisshaar, J. C. *J. Phys. Chem.* **1989**, *93*, 1963.

(4) Elkind, J. L.; Armentrout, P. B. *J. Phys. Chem.* **1986**, *90*, 5736; *J. Am. Chem. Soc.* **1986**, *108*, 2765.

(5) Elkind, J. L.; Armentrout, P. B. *J. Phys. Chem.* **1986**, *90*, 6576.

(6) Elkind, J. L.; Armentrout, P. B. *J. Phys. Chem.* **1987**, *91*, 2037 and references therein.

(7) Sunderlin, L. S.; Armentrout, P. B. *J. Phys. Chem.* **1988**, *92*, 1209.

(8) van Koppen, P. A.; Beauchamp, J. L.; Dearden, D. V.; Bowers, M. T., to be published.

(9) Johnsen, R.; Castell, F. R.; Biondi, M. A. *J. Chem. Phys.* **1974**, *61*, 5404.

(10) The technique of surface ionization also allows production of known amounts of low-lying excited states; see ref 7.

(11) Kemper, P. R.; Bowers, M. T. *J. Am. Soc. Mass Spectrom.*, in press.

0002-7863/90/1512-3231$02.50/0

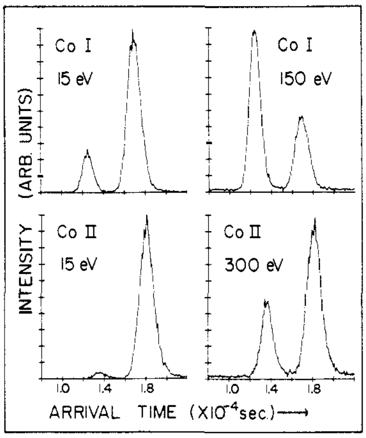

Figure 1. Arrival-time distribution of Co^+ in He; $P_{He} \simeq 1.0$ Torr, T = 160 K for $CoCO_3NO$ (I) and $CoCp(CO)_2$ (II). The shift in arrival time between I and II is due to slightly different E/N values in the experiments. The times shown include time in the quadrupole, which must be subtracted to determine the mobility.

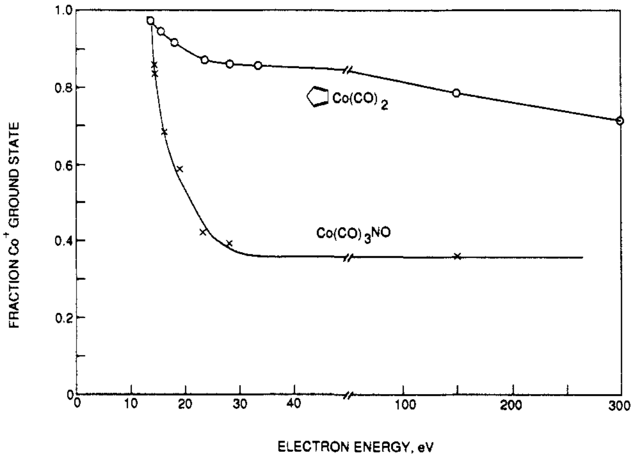

Figure 2. Percent Co^+ ground state versus ionizing energy. Note change in energy axis at 50 eV.

distribution of times between injection and collection forms the arrival-time distribution. Total time between ion formation and collection is 100–400 μs. No ions other than Co^+ and $Co{\cdot}He^+$ ($\lesssim 1\%$) were observed after the reaction cell.

Figure 1 shows the ATDs for Co^+ formed from I and II. In both cases, two peaks are observed and the peak at longer time (lower mobility) increases with decreasing ionizing energy, approaching 100% at ~14 eV. Figure 2 shows the percent slower peak versus ionizing energy. An unlikely explanation is the formation of another ion with the same nominal mass which could not be differentiated in the quadrupole. The m/e 59 peak was examined at high resolution, and no such ion was found. We are convinced that the peaks are due to ground-state $Co^+(3d^8,{}^3F)$ and a metastable excited state, probably $Co^+(3d^74s^1,{}^3F)$. The respective zero field reduced mobilities[12] were measured to be $K_0 = 16.2 \pm 2$ cm^2/(V s) (ground state) and $K_0 = 24.1 \pm 2$ cm^2/(V s) (excited state); their ratio is 1.485 ±0.05. No variation in K_0 was found between cell temperatures of 160 and 300 K.

If Co^+ electronic states are responsible for the different mobilities, the increased mobility of the ^3F state is probably due to the populated 4s orbital. The 4s orbital is considerably larger than the 3d;[2,13] thus, long-range repulsion between Co^+ and He should increase if it is occupied. This will reduce the effective attractive potential due to the charge-induced dipole, lowering the collision rate. Tonkyn et al.[2] have used this argument to help explain metal ion/alkane clustering data. Mobilities in helium are often determined largely by forces other than the charge-induced dipole, due to the small polarizability of helium.[12,14] The existing Ti^+ mobility data[9] support the above hypothesis. The Ti^+ ground state $(3d^24s^1,{}^4F)$ includes a 4s electron[6] and has a mobility of 25.5 ± 0.5 cm^2/(V s),[9] very similar to that of the excited-state cobalt. This may indicate that configuration (not electronic state) determines mobility. Further support for long-range repulsion between excited Co^+ and He comes from the absence of deactivation in collisions with helium ($k < 1 \times 10^{-14}$ cm^3/s). Deactivation might be expected in an intimate collision. We are examining other first-row transition metals to check the correlation between high mobility and occupied 4s orbital.

Finally, we can compare the apparent effects of 3d and 4s orbital population on ion mobility. Potassium ions $(3p^6,{}^1S)$ have a mobility of He of 21.6 cm^2/(V s).[14,15] If the metal ion/He interaction were purely electrostatic (i.e., charge-induced-dipole attraction versus electron–electron repulsion), we would expect that adding 3d electrons to K^+ should cause some increase in mobility due to increased electron density on the ion while adding a 4s electron should cause a greater increase.[16] In fact, the 3d electrons cause a large *decrease* in mobility (at least for ground-state Co^+), indicating a decreased repulsion, which must be due to other factors. Studies of other first row transition metal ions are in progress.

Acknowledgment. National Science Foundation support under Grant CHE88-17201 is gratefully acknowledged.

---

(12) McDaniel, E. W.; Mason, E. A. *The Mobility and Diffusion of Ions in Gases*; Wiley: New York, 1973; p 6.

(13) Huheey, J. E. *Inorganic Chemistry*; Harper and Row: New York, 1972; pp 40–43.

(14) Lindinger, W.; Albritton, D. L. *J. Chem. Phys.* **1975**, *62*, 3517.

(15) Ellis, H. W.; et seqq. Transport Properties of Gaseous Ions Over a Wide Range. *At. Nucl. Data Tables* **1976**, *17*, 177; **1978**, *22*, 179; **1984**, *31*, 113.

(16) Electron density at 2.5 Å in Co^+ increases by 7.5 when a 4s electron is added (see ref 2).

Structural Studies by $^1H/^{13}C$ Two-Dimensional and Three-Dimensional HMQC–NOE at Natural Abundance on Complex Carbohydrates

P. de Waard, R. Boelens,* G. W. Vuister, and
J. F. G. Vliegenthart

Department of Chemistry, University of Utrecht
Padualaan 8, 3584 CH Utrecht, The Netherlands

Received October 3, 1989

Studies on the chain conformation of oligosaccharides are mainly restricted to analysis of NOE spectra to estimate the torsion angles defining the glycosidic linkages.[1,2] A major problem in the analysis is the overlap of resonances in the bulk region between 3 and 4 ppm. Recently, we demonstrated a homonuclear 3D NOE–HOHAHA experiment to resolve overlap in 2D NOE spectra of oligosaccharides.[3] ^{13}C spectra of oligosaccharides are much better resolved than ^1H spectra. Therefore, the inclusion or addition of a ^{13}C frequency domain is a promising extension of 2D ^1H NOE spectroscopy. So far heteronuclear NMR experiments such as 2D and 3D HMQC–NOE have been limited to isotope-enriched proteins.[4-9] Furthermore, $^1H/^{13}C$ HMQC–

---

(1) Carver, J. P.; Brisson, J. R. *Biology of Carbohydrates*; Wiley: New York, 1984; pp 289–331.

(2) Homans, S. W.; Dwek, R. A.; Rademacher, T. W. *Biochemistry* **1987**, *26*, 6571–6578.

(3) Vuister, G. W.; De Waard, P.; Boelens, R.; Vliegenthart, J. F. G.; Kaptein, R. *J. Am. Chem. Soc.* **1989**, *111*, 772–774.

(4) Fesik, S. W.; Zuiderweg, E. R. P. *J. Magn. Reson.* **1988**, *78*, 588–593.

(5) Fesik, S. W.; Luly, J. R.; Erickson, J. W.; Abad-Zapatero, C. *Biochemistry* **1988**, *27*, 8297–8301.

(6) Shon, K.; Opella, S. J. *J. Magn. Reson.* **1989**, *82*, 193–197.

(7) Marion, D.; Kay, L. E.; Sparks, S. W.; Torchia, D. A.; Bax, A. *J. Am. Chem. Soc.* **1989**, *111*, 1515–1517.

0002-7863/90/1512-3232$02.50/0